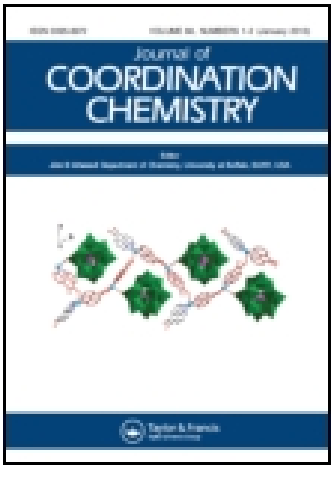

Journal of Coordination Chemistry
Publication details, including instructions for authors and subscription information:
http://www.tandfonline.com/loi/gcoo20

Synthesis and characterization of a pair of temperature and cosolvent-dependent Zn(II)-organic frameworks containing a novel discrete single-walled Zn(II)-organic coordination polymer nanotube

Kou-Lin Zhang[a], Chu-Yue Jing[a], Ye Deng[a], Lei Zhang[a], Qing-Hua Meng[b], Pei-Zhi Zhu[a] & Seik Weng Ng[c]

[a] Key Laboratory of Environmental Material and Environmental Engineering of Jiangsu Province, College of Chemistry and Chemical Engineering, Yangzhou University, Yangzhou, China

[b] Jiangsu Key Laboratory of Green Synthesis for Functional Materials, Jiangsu Normal University, Xuzhou, China

[c] Department of Chemistry, University of Malaya, Kuala Lumpur, Malaysia

Accepted author version posted online: 28 May 2014.Published online: 12 Jun 2014.

To cite this article: Kou-Lin Zhang, Chu-Yue Jing, Ye Deng, Lei Zhang, Qing-Hua Meng, Pei-Zhi Zhu & Seik Weng Ng (2014) Synthesis and characterization of a pair of temperature and cosolvent-dependent Zn(II)-organic frameworks containing a novel discrete single-walled Zn(II)-organic coordination polymer nanotube, Journal of Coordination Chemistry, 67:9, 1596-1612, DOI: 10.1080/00958972.2014.926006

To link to this article: http://dx.doi.org/10.1080/00958972.2014.926006

Journal of Coordination Chemistry, 2014
Vol. 67, No. 9, 1596–1612, http://dx.doi.org/10.1080/00958972.2014.926006

Synthesis and characterization of a pair of temperature and cosolvent-dependent Zn(II)-organic frameworks containing a novel discrete single-walled Zn(II)-organic coordination polymer nanotube

KOU-LIN ZHANG*†, CHU-YUE JING†, YE DENG†, LEI ZHANG†, QING-HUA MENG‡, PEI-ZHI ZHU**† and SEIK WENG NG§

†Key Laboratory of Environmental Material and Environmental Engineering of Jiangsu Province, College of Chemistry and Chemical Engineering, Yangzhou University, Yangzhou, China
‡Jiangsu Key Laboratory of Green Synthesis for Functional Materials, Jiangsu Normal University, Xuzhou, China
§Department of Chemistry, University of Malaya, Kuala Lumpur, Malaysia

(*Received 12 August 2013; accepted 1 April 2014*)

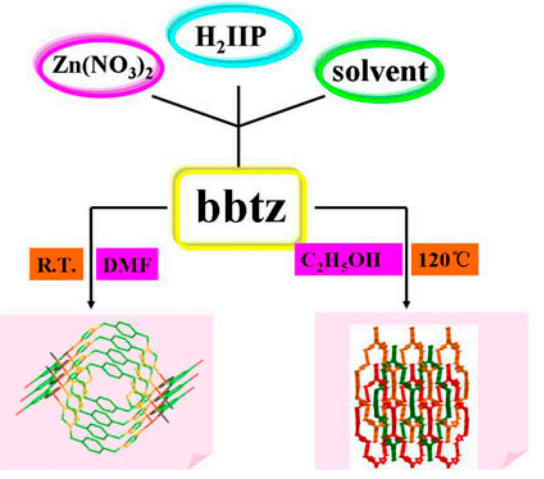

The temperature and the cosolvent have great influence on the engineering of crystalline architectures of a pair of Zn(II)-organic frameworks with H_2IIP and bbtz: the novel discrete single-walled Zn(II)-organic coordination polymer nanotube **1** and an interesting 3-D polycatenated array of layers **2**. The dehydrated SWCPNT-**1** exhibits reversible dehydration and rehydration from ambient air.

*Corresponding authors. Email: klzhang@yzu.edu.cn (K.-L. Zhang); pzzhu@yzu.edu.cn (P.-Z. Zhu)

A pair of temperature and cosolvent-controlled assemblies of one dimensional (1-D) and two dimensional (2-D) Zn(II)-organic frameworks (ZOFs] based on 5-iodoisophthalic acid (H_2IIP) and an auxiliary flexible ligand, 1,4-bis(triazol-1-ylmethyl)benzene (bbtz) with different structures, has been rationally designed and successfully synthesized. Results show that when the reaction was carried out under ambient condition, the novel discrete single-walled Zn(II)-organic coordination polymer nanotube $\{[Zn(IIP)(bbtz)(H_2O)]\cdot H_2O\}_n$ (SWCPNT-**1**), which shows a fascinating 3-D supramolecular interdigitated columnar microporous architecture supported by face to face $\pi\cdots\pi$ stacking interactions and hydrogen bonds, was generated, whereas under solvothermal condition at 120 °C, an interesting 3-D-polycatenated array of layers, [Zn(IIP)(bbtz)] (**2**), which further extends into a threefold-interpenetrated 3-D supramolecular mesoporous framework with 1-D channels (*ca.* 3.46×1.54 nm^2) through C–I···O halogen bonds would be obtained. Interestingly, the reversible *in situ* rapid rehydration from static air is significantly observed in the discrete SWCPNT-**1**, revealing its potential application as water absorbent and sensing material. The dehydrated SWCPNT-**1** shows selective gas adsorption of CO_2 over N_2. Luminescent studies show that SWCPNT-**1**, dehydrated SWCPNT-**1,** and **2** exhibit blue fluorescence in the solid state. The water molecules in SWCPNT-**1** affect its fluorescent property.

Keywords: Synthesis; Nanotubular metal–organic framework; Characterization; Property

1. Introduction

Since the discovery of carbon nanotubes in 1991 [1], many nanotubular structures including inorganic nanotubes containing elements other than carbon and organic nanotubes have been synthesized [2–6]. Recently, significant progress has been made in the design and synthesis of nanotubular metal–organic frameworks (MOFs) based on coordinative bonds because these porous nanotubular MOFs have fascinating structures and potential applications in gas storage, sensors, and other technologies. Although many MOFs with open channels have been synthesized [7–11], only a few nanotubular MOFs have been reported. However, the nanotubes in the reported nanotubular MOFs were normally assembled into high 3-D frameworks through further interconnection or interweaving of the nanotubular units by the multidentate ligands [12–18]. The discrete 1-D coordination polymer nanotubes (CPNTs) are still very limited [19–32]. Therefore, it is a particularly challenging subject to design and construct discrete CPNTs. It is well known that the architectures of MOFs can be controlled and modulated by selecting the coordination geometry of metal nodes, the chemical nature of the ligand, counter ions, and a number of experimental variables such as the solvent, templates, pH, and the reaction temperature [33–45]. It has been proved that organic aromatic polycarboxylates, as well as flexible triazole ligands, are good building blocks for the construction of coordination polymers and multidimensional supramolecular networks [46–51]. It is worthy to mention that the temperature-controlled supramolecular assembly in MOFs has received relatively little attention [52].

From a design perspective, to assemble 1-D discrete CPNTs, the linking mode of the organic ligand should meet with the coordination geometry of the metal nodes. Some strategies have been used to construct discrete CPNTs. For example, it has been reported that the 0-D squares are connected from the four vertexes by a bridging organic ligand to generate 1-D interpenetrating or non-interpenetrating multi-walled discrete CPNTs [19, 20]. Previously, we had successfully obtained an unprecedented discrete single-walled Zn(II)-organic tube with 5-iodoisophthalate in the presence of btp as auxiliary ligand (the internal dimensions: $0.92 \times 0.90\ nm^2$), in which the 0-D elliptical dimeric subunit is found [53]. So, we think it may be an effective strategy that the metal ions with d^{10} configuration are firstly

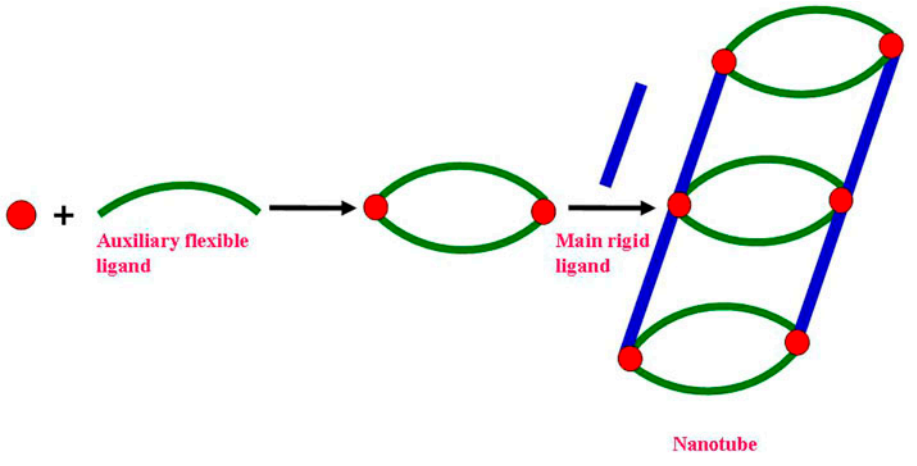

Chart 1. Construction of the discrete SWCPNT.

connected by auxiliary flexible organic ligand with appropriate length and intramolecular interdigitated angle to generate a nanosized elliptical dimeric subunit, and then the main rigid organic ligand links the elliptical subunits from two vertexes to generate a discrete single-walled coordination polymer nanotube (SWCPNT) (chart 1). However, the connection of the 0-D nanosized elliptical dimeric unit to generate discrete single-walled Zn(II)-organic nanotube has not been explored prior to the present report.

Along this line, we chose H_2IIP to assemble with Zn(II) ion in the presence of the auxiliary ligand bbtz at different reaction temperature, which is based chiefly on the following considerations. (1) The I group is a potential interaction site for creating C–I···N/O/I halogen bonds which may help to extend the linkage into high dimensional supramolecular framework due to their specific directional nature and relatively high halogen bonding energy [54]. (2) The auxiliary flexible ligand bbtz usually has two different conformations: *trans-gauche (TG)* and *gauche-gauche (GG)* [55]. So, its coordination conformations may easily be influenced by temperature. Furthermore, the auxiliary flexible ligand bbtz is much longer than 1,3-bis(1,2,4-triazol-1-yl)propane (btp). The *GG* conformation of bbtz has the potential to form nanosized elliptical dimeric unit with Zn(II) node, which can further be connected by the rigid ligand IIP^{2-}, resulting in the discrete single-walled Zn(II) coordination polymer nanotube. Thus, a structural prediction of the resulting framework may be possible to some extent (scheme 1).

Based on this strategy, we have successfully obtained a pair of temperature and cosolvent-controlled Zn(II)-organic frameworks (ZOFs): a novel discrete single-walled Zn(II)-organic coordination polymer nanotube, $\{[Zn(IIP)(bbtz)(H_2O)]\cdot H_2O\}_n$ (SWCPNT-**1**), that is further extended to a "soft" 3-D interdigitated supramolecular columnar microporous framework via weak contacts, and an interesting 3-D-polycatenated array of layers, [Zn(IIP)(bbtz)] (**2**), which further extends into a novel threefold-interpenetrated 3-D supramolecular mesoporous framework with 1-D channels (*ca.* $3.46 \times 1.54\ nm^2$) through C–I···O halogen bond, were obtained at room temperature and under solvothermal condition at 120 °C, respectively. The freedom of C–C and C–N single σ-bond rotation in the bbtz ligand gives rise to variable conformations (scheme 2), which are mainly responsible for the different architectures of SWCPNT-**1** and **2**. The thermal stability and solid-state fluorescent

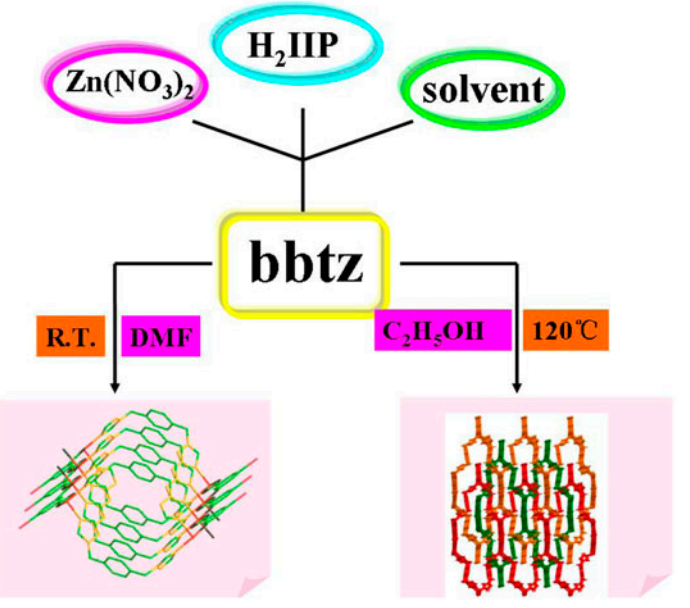

Scheme 1. Simplified representation of the aqueous medium synthesis with architectures of SWCPNT-**1** and **2**, showing that the temperature and cosolvent have great effect on the supramolecular assemblies.

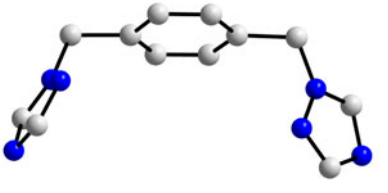

GG (*gauche-gauche*), bbtz in SWCPNT-**1**

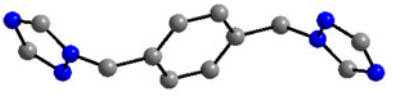

TG (*trans-gauche*), bbtz in **2**

Scheme 2. The conformations of the auxiliary ligand bbtz in SWCPNT-**1** and **2**.

properties have been studied. The water molecules affect the fluorescent intensity of SWCPNT-**1** greatly. Interestingly, SWCPNT-**1** shows rapid and reversible dehydration–rehydration in the air. The gas sorption was performed.

2. Experimental section

2.1. *Materials and characterization*

The starting materials, H_2IIP and bbtz, were prepared according to the previously reported procedures [53, 56]. The other reagents were purchased commercially and used without further purification. Elemental analyses (C, H, and N) were carried out on a 240 °C Elemental analyzer. FT-IR spectra (4000–400 cm^{-1}) were recorded from KBr pellets in Magna 750 FT-IR spectrophotometer. The solid-state fluorescence emission spectra were recorded using an F-4500 Fluorescence spectrophotometer (Hitachi). Both the excitation and emission pass width are 5.0 nm. X-ray powder diffraction data were collected on a computer-controlled Bruker D8 Advanced XRD diffractometer equipped with Cu-Kα monochromator ($\lambda = 1.5418$ Å) at a scanning rate 0.02° s^{-1} from 5° to 50°. The sorption experiments for gasses and vapors were measured with an automatic gravimetric adsorption apparatus (Magnetic Suspension Balances, Rubotherm Ltd, Germany) at 278.15 K. The initial outgassing process for the sample was carried out under a high vacuum at 378.15 K for *ca*. 4 h.

2.2. *Synthesis of complexes*

2.2.1. Synthesis of $[Zn(IIP)(bbtz)(H_2O)]\cdot H_2O$ (SWCPNT-1). A mixture of H_2IIP (0.029 g, 0.1 mM) and NaOH (0.004 g, 0.1 mM) was dissolved in *N*,*N*′-dimethylformamide (DMF) (5 mL) and then an aqueous solution of $Zn(NO_3)_2\cdot 6H_2O$ (0.029 g, 0.1 mM) in water (5 mL) was added whilst stirring. To this solution, bbtz (0.024 g, 0.1 mM) in water (5 mL) was added and then filtered. The filtrate was kept at ambient temperature for several days and yellow block crystals were formed (yield: 65% based on H_2IIP). Anal. Calcd for $C_{20}H_{19}IN_6O_6Zn$: C, 38.02; H, 3.03; N, 13.30. Found: C, 37.89; H, 2.91; N, 13.51%. IR/cm^{-1} (KBr): 3365(m), 3127(w), 1661(vs), 1609(vs), 1552(s), 1428(s), 1373(vs), 1283 (m), 1122(m), 1101(m), 990(m), 730(s).

2.2.2. Synthesis of $[Zn(IIP)(bbtz)]_n$ (2). A mixture containing $Zn(NO_3)_2\cdot 6H_2O$ (0.029 g, 0.1 mM), NaOH (8 mg, 0.2 mM), H_2IIP (29.2 mg, 0.1 mM), bbtz (0.024 g, 0.1 mM), water (3 mL), and ethanol (3 mL) was sealed in a Teflon reactor, which was heated at 120 °C for three days and then it was cooled to room temperature at 10 °C h^{-1}. Red needle crystals were collected (yield: 70% based on H_2IIP). Anal. Calcd for $C_{20}H_{15}IN_6O_4Zn$: C, 40.32; H, 2.54; N, 14.11 Found: C, 40.28; H, 2.41; N,13.89%. IR/cm^{-1} (KBr): 3060(s), 1615(vs), 1548(s), 1424(s), 1343(vs), 1282(s), 1140(s), 999(m), 773(m), 731(s), 673(s).

2.3. *X-ray single-crystal structure determination*

Crystallographic data were collected at 296(2) K with a Siemens SMART CCD diffractometer using graphite-monochromated (Mo Kα) radiation ($\lambda = 0.71073$ Å), ψ and ω scans mode. The structures were solved by direct methods and refined by full-matrix least-squares on F^2 method using SHELXL-97 program [57]. Intensity data were corrected for Lorenz and polarization effects and a multi-scan absorption correction was performed. Generally, the positions of C-bound H atoms were generated on idealized geometries. The H atoms of water were uniquely located in different Fourier maps and then kept fixed. All non-hydrogen atoms were refined anisotropically. The contribution of the hydrogen atoms was

included in the structure factor calculations. It should be mentioned that the "ALERT level **A**" problem in the checkcif/platon report of **SWCPNT-1** indicates that this structure contains large solvent accessible voids even if both the lattice and coordinated water molecules are included, which can further be verified by thermogravimetric analysis (TGA). Furthermore, from crystallographic point of view, there is nothing to do with the voids. Details of crystal data, collection, and refinement are listed in table 1.

3. Results and discussion

3.1. *Syntheses of the complexes*

A pair of Zn(II)-organic frameworks, SWCPNT-**1** and **2**, was prepared at room temperature and under solvothermal condition at 120 °C, respectively. Interestingly, the molar ratio of H_2IIP: NaOH is very important for the growth of single crystals. The molar ratios of H_2IIP : NaOH (1 : 1 for 1 and 1 : 2 for 2, respectively) were used when we tried to synthesize SWCPNT-**1** and **2**. Otherwise, the polycrystals or cotton-like solids were obtained. It should be mentioned that SWCPNT-**1** and **2** cannot be obtained without the presence of slightly quantity of DMF and ethanol, respectively, which indicates that the temperatures, as well as

Table 1. Crystal data and structure refinement for SWCPNT-**1** and **2**.

	SWCPNT-**1**	**2**
Empirical formula	$C_{20}H_{19}IN_6O_6Zn$	$C_{20}H_{15}IN_6O_4Zn$
Formula weight	631.68	595.65
Temperature (K)	296(2)	296(2)
Wavelength (Å)	0.71073	0.71073
Crystal system	Triclinic	Monoclinic
Space group	*P-1*	*P*2(1)/*c*
a (Å)	10.2284(15)	15.3544(13)
b (Å)	10.6481(15)	14.6663(13)
c (Å)	13.932(2)	10.2442(9)
α (°)	72.386(2)	90
β (°)	86.794(2)	108.0450(10)
γ (°)	72.740(2)	90
V (Å^3)	1380.2(3)	2193.4(3)
Z	2	4
D_{Calcd} (Mg m^{-3})	1.520	1.804
Absorption coeff (mm^{-1})	2.050	2.567
F (0 0 0)	624	1168
θ Range for data collection (°)	1.53–25.00	1.97–27.56
Index ranges	$-12 \le h \le 12$	$-19 \le h \le 19$
	$-11 \le k \le 12$	$-18 \le k \le 19$
	$-13 \le l \le 16$	$-12 \le l \le 13$
Reflections collected	9600	19,020
Unique (R_{int})	4797 [R(int) = 0.0426]	5037 [R(int) = 0.0262]
Completeness to $\theta = 27.5$	98.6%	99.3%
Max. and min. transmission	0.735 and 0.546	0.680 and 0.468
Goodness-of-fit on F^2	1.101	1.062
Final R indices [$I > 2\sigma(I)$]	$R_1 = 0.0768$	$R_1 = 0.0320$
	$wR_2 = 0.2370$	$wR_2 = 0.0948$
R indices (all data)	$R_1 = 0.1378$	$R_1 = 0.0420$
	$wR_2 = 0.2811$	$wR_2 = 0.1014$
Largest diff. peak and hole (e Å^{-3})	2.262 and −1.445	1.614 and −0.308

cosolvents have great influence on the crystal growth for some MOFs. All the carboxylate groups in SWCPNT-**1** and **2** are found to be deprotonated as supported by the data of FT-IR spectroscopy and the results of crystallographic analysis (see below). There are great differences in the coordination modes of the auxiliary flexible ligand bbtz (scheme 2), which exert a significant influence on the crystalline architectures as described below.

3.2. *Crystal structure descriptions*

3.2.1. Structural description of $\{[Zn(IIP)(bbtz)(H_2O)]\cdot H_2O\}_n$ (SWCPNT-1). The work presented here reports a convenient one-pot synthesis of one novel discrete infinite SWCPNT-**1** (scheme 3), which is obtained under "soft" ambient condition. To the best of our knowledge, SWCPNT-**1** is the unique discrete single-walled Zn(II)-organic coordination polymer nanotube.

Single-crystal X-ray diffraction analysis reveals that SWCPNT-**1** crystallizes in the triclinic system with space group *P-1* and has an interesting discrete nanotubular chain structure. The asymmetric unit of SWCPNT-**1** consists of one independent Zn(II) ion, one IIP^{2-} ligand, one bbtz ligand, one coordinated water molecule, and one lattice water molecule [figure 1(A)]. The central Zn atom adopts distorted octahedral coordination geometry

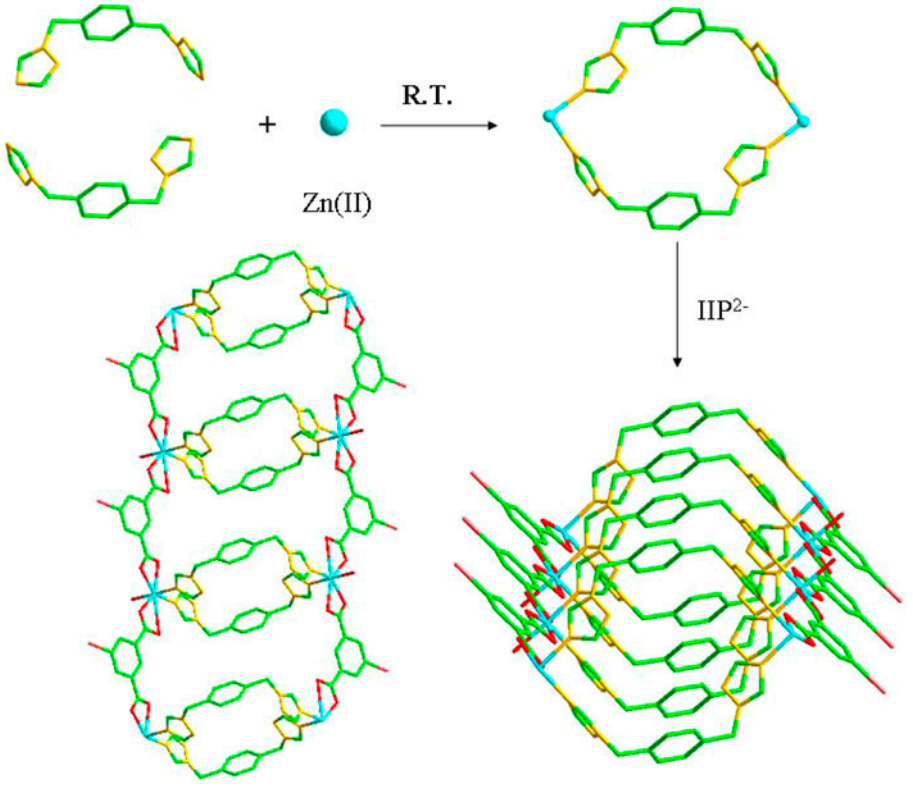

Scheme 3. Synthesis of the discrete single-walled Zn(II)-organic coordination polymer nanotube SWCPNT-**1**.

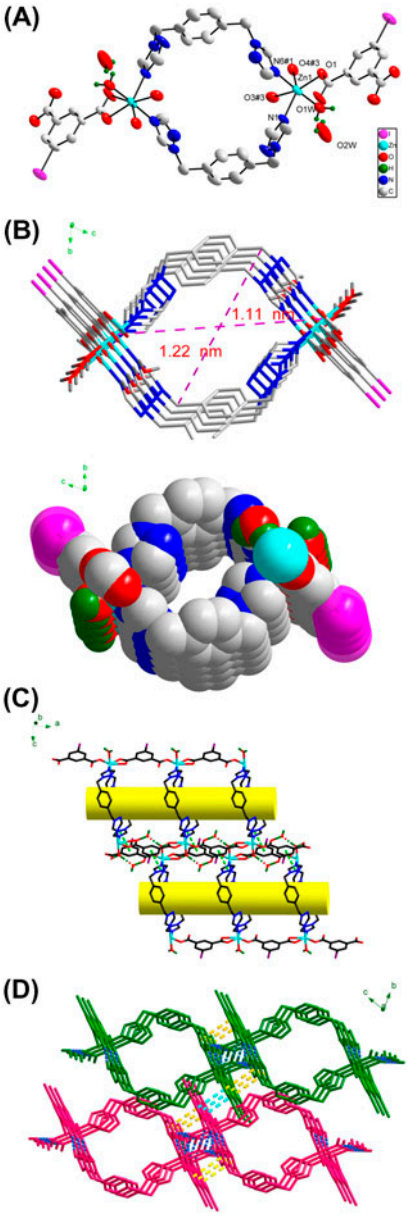

Figure 1. (A) The coordination environment of Zn(II) and the elliptical dimeric metallamacrocycle ring in SWCPNT-**1** (#1 $-x+2,-y,-z+2$; #3 $x+1$, y, z). (B) (Top) The dimensions of SWCPNT-**1** showing the lattice waters reside just in the wall of the tube, (Bottom) Space-filling diagram of the nanotube, showing the large cavity even including the lattice waters. (C) 2-D supramolecular layer formed through O–H···O hydrogen bonds and $\pi\cdots\pi$ stacking interactions between the discrete nanotubes with a stick inside. (D) 2-D supramolecular layer stacks through O–H···O hydrogen bonds and $\pi\cdots\pi$ stacking interactions to generate a 3-D supramolecular interdigitated columnar microporous framework.

through bonding to three O-donors from two IIP^{2-} ligands, two triazole N-donors from two bbtz ligands, and one O donor from the coordinated water molecule (table 2). Two bbtz

ligands coordinate to two Zn(II) ions to form an elliptical dimeric metallamacrocycle ring [$Zn(bbtz)_2Zn$], and the rings thus created are then further linked with each other through IIP^{2-} ligands in (k^2)-(k^1)-μ_2 fashion to form a novel discrete 1-D elliptical SWCPNT [figure 1(B), scheme 3]. The auxiliary ligand bbtz adopts *GG* conformation [16] and has a larger intramolecular N1···N6 distance [9.296(12) Å] and a bigger bent angle between two triazole rings (67.90°), which results in the formation of nanotubular chain structure. The nanotube lies parallel to the crystallographic *a*-axis and has an internal dimension of *ca*. 1.22 × 1.11 nm^2. It should be noted that calculations using PLATON [58] based on the crystal structure show that the total solvent-accessible volume is 298.0 $Å^3$ per unit cell, even including both the lattice water and coordinated water molecules, comprising 21.6% of the crystal volume. If both the lattice water and coordinated water molecules were excluded, the total solvent-accessible volume reaches 378.0 $Å^3$ per unit cell, comprising 27.4% of the crystal volume.

Just in the wall of the coordination polymer nanotube lies one-ordered interstitial H_2O molecule. Both the interstitial water molecule and the coordinated one further assemble into a discrete water dimer. The O1W and O2W form hydrogen bonds with both the coordinated and uncoordinated carboxylate oxygen atoms of the neighboring tubes [O1W–H1W1···O3 (2.722 Å) and O2W–H2W1···O2 (2.720 Å)] [figure 1(C)]. Thus, the nanotubes are aligned into a 2-D columnar sheet, likely driven by such O–H···O hydrogen bonds and $\pi\cdots\pi$ stacking interactions between the benzene and triazole rings of the adjacent tubes evidenced by the centroid···centroid distance of 3.895 Å. The 2-D supramolecular layer was further linked each other through face to face $\pi\cdots\pi$ stacking interactions between two benzene rings of the adjacent tubes, ultimately resulting in the formation of a fascinating 3-D supramolecular interdigitated columnar microporous framework [figure 1(D)]. The Ow···Ow distance (2.805 Å) in the discrete water dimer is comparable to that for the ice II phase (2.77–2.84 Å) [59].

3.2.2. Structural descriptions of the crystalline polymer $[Zn(IIP)(bbtz)]_n$ (2). Complex **2** is obtained solvothermally and crystallizes in the monoclinic system with space group $P2_1/c$. It exhibits an interesting 3-D-polycatenated array of layers, in which every layer is catenated with the two neighboring atoms, up and down. The asymmetric unit of **2** consists of one Zn(II) atom, one IIP^{2-}, and one bbtz ligand [figure 2(A)].

Table 2. Selected bond lengths [Å] and angles [°] for SWCPNT-**1** and **2**.

SWCPNT-**1**			
Zn(1)–O(1)	2.037(8)	Zn(1)–N(6)#1	2.117(12)
Zn(1)–O(1W)	2.078(10)	Zn(1)–N(1)	2.129(9)
Zn(1)–O(4)#3	2.117(8)	Zn(1)–O(3)	2.528(3)
O(1)–Zn(1)–O(1W)	86.7(4)	O(4)#3–Zn(1)–N(6)#1	87.7(4)
O(1)–Zn(1)–O(4)#3	95.7(3)	O(1)–Zn(1)–N(1)	126.7(4)
O(1W)–Zn(1)–O(4)#3	90.0(4)	O(1 W)–Zn(1)–N(1)	90.4(4)
O(1)–Zn(1)–N(6)#1	92.0(4)	O(4)#3–Zn(1)–N(1)	137.5(3)
O(1W)–Zn(1)–N(6)#1	177.3(4)	N(6)#1–Zn(1)–N(1)	92.3(4)
Complex **2**			
Zn(1)–O(1)	1.970(2)	Zn(1)–N(1)	2.015(4)
Zn(1)–O(3)#2	1.970(3)	Zn(1)–N(4)	2.020(3)
O(3)–Zn(1)–O(1)	102.82(11)	O(3)–Zn(1)–N(4)	113.47(14)
O(3)–Zn(1)–N(1)	114.12(14)	O(1)–Zn(1)–N(4)	110.89(13)
O(1)–Zn(1)–N(1)	108.15(13)	N(1)–Zn(1)–N(4)	107.28(14)

Note: Symmetry transformations used to generate equivalent atoms: #1 $-x+2$, $-y$, $-z+2$ #3 $x+1$, y, z for SWCPNT-**1**; #2 x, y, $z-1$ for **2**.

Each Zn(II) atom is tetracoordinated by two nitrogen atoms from two bridging bbtz ligands and two oxygen atoms from two individual IIP^{2-} ligands, showing a distorted tetrahedral coordination geometry with the bond angles around each Zn(II) atom vary from 102.83(12)° and 114.11(14)° (table 2). The auxiliary flexible ligand bbtz adopts *TG* conformation (scheme 2) and links the adjacent Zn(II) ions to form a 1-D *zig–zag* chain with the pitches of 15.597(1) Å [figure 2(B)]. Notably, the main rigid ligands IIP^{2-} are almost perpendicular to the 1-D motifs. The parallel *zig–zag* chains are bridged by the IIP^{2-} linkages in bismonodentate (k^1)-(k^1)-μ_2 coordination fashion, leading to the formation of a novel 3-D-polycatenated array of layers with wave-like nanoporous sheet with (4, 4) topology [14.7655(10) × 10.2442(9) $Å^2$] [figure 2(C) and (D)] [60]. These 3-D-polycatenated array of layers are further extended to a fascinating threefold-interpenetrated 3-D supramolecular network with 1-D mesoporous channel (*ca*. 3.46 × 1.54 nm^2) along [0 0 1] direction via C–I···O halogen bonds [3.4925 Å] [figure 2(E) and (F)].

3.3. *FT-IR spectra and thermogravimetric analyses*

The FT-IR spectral data show features attributable to the carboxylate stretching vibrations of both SWCPNT-**1** and **2**. The absence of bands in the range of 1680–1760 cm^{-1} indicates the complete deprotonation of H_2IIP in these two complexes. The characteristic bands of the carboxylate groups appear in the range 1552–1598 cm^{-1} for the asymmetric stretching and 1384–1490 cm^{-1} for the symmetric stretching. In the FT-IR spectra of SWCPNT-**1**, the broad band centered around 3300 cm^{-1} corresponds to the –OH stretching vibrations of the water molecules [61].

To examine the thermal stability of SWCPNT-**1** and **2**, the TGA was performed on polycrystalline samples under a nitrogen atmosphere in flowing N_2 with a heating rate of 10 °C min^{-1} (figure 3). For SWCPNT-**1**, the weight decrease of 5.18% from 63 to 105 °C corresponds to the escape of both the interstitial and coordinated water molecules (Calcd 5.69%). The second step starts from 120 °C and ends at 215 °C with a weight loss of 9.53%, which may possibly be attributable to the loss one triazol ring in the bbtz ligand (Calcd 10.29%). A sharp weight loss beginning at 316 °C indicates decomposition of the host tube.

No weight loss is observed below 320 °C in the TG curve of **2**, which further confirms the absence of the lattice water molecules in the phase. Complex **2** decomposes at 320 °C, revealing that **2** has high framework stability.

3.4. *Removal and reintroduction of water in SWCPNT-1*

TGA shows clearly that both the interstitial and coordinated water molecules in SWCPNT-**1** could be excluded upon heating. To study the dehydration–rehydration property of SWCPNT-**1**, the *in situ* variable temperature powder X-ray diffraction (PXRD) was performed at room temperature, 105 °C, and then room temperature again upon cooling down the dehydrated material automatically just in static air (figure 4). Remarkably, the PXRD patterns clearly show that SWCPNT-**1** undergoes reversible dehydration and rehydration upon exposure of the dehydrated material just in static air, the dehydrated phase rehydrates rapidly, resulting in the re-establishment of the original crystal structure upon cooling to room temperature. This is further verified by the TG analysis of the rehydrated material of SWCPNT-**1** [the first step mass loss corresponding to water molecules in TGA: 5.03%

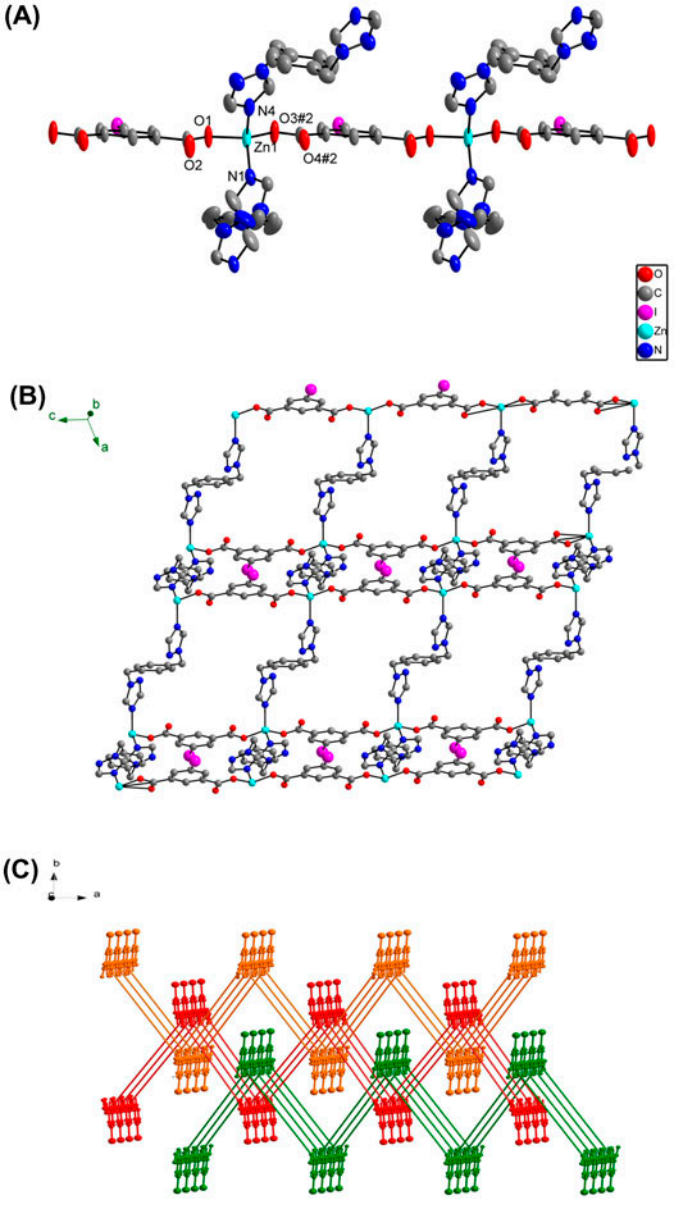

Figure 2. (A) View of the coordination environment of Zn(II) and the coordination mode of IIP^{2-} in **2** (symmetry code: #2 x, y, $z-1$); (B) Perspective view of the wave-like 2-D coordination layer; (C) Schematic representation of the 3-D polycatenated array of layers. The bbtz linkers are simplified as rods for clarity. Each layer is catenated with the two neighboring, up and down; (D) Space-filling view of the threefold interpenetrated 3-D supramolecular network, considering the C–I···O bonds; (E) Schematic view of the threefold interpenetrated 3-D supramolecular network, where the blue dashed lines represent the C–I···O bonds; (F) Size of the channel (see http://dx.doi.org/10.1080/00958972.2014.926006 for color version).

(Calcd 5.69%) (see figure S1, see online supplemental material at http://dx.doi.org/10.1080/00958972.2014.926006)]. It should be pointed out that the dehydrated phase of SWCPNT-**1** still remains integrated after the water molecules are lost, but the structure of the

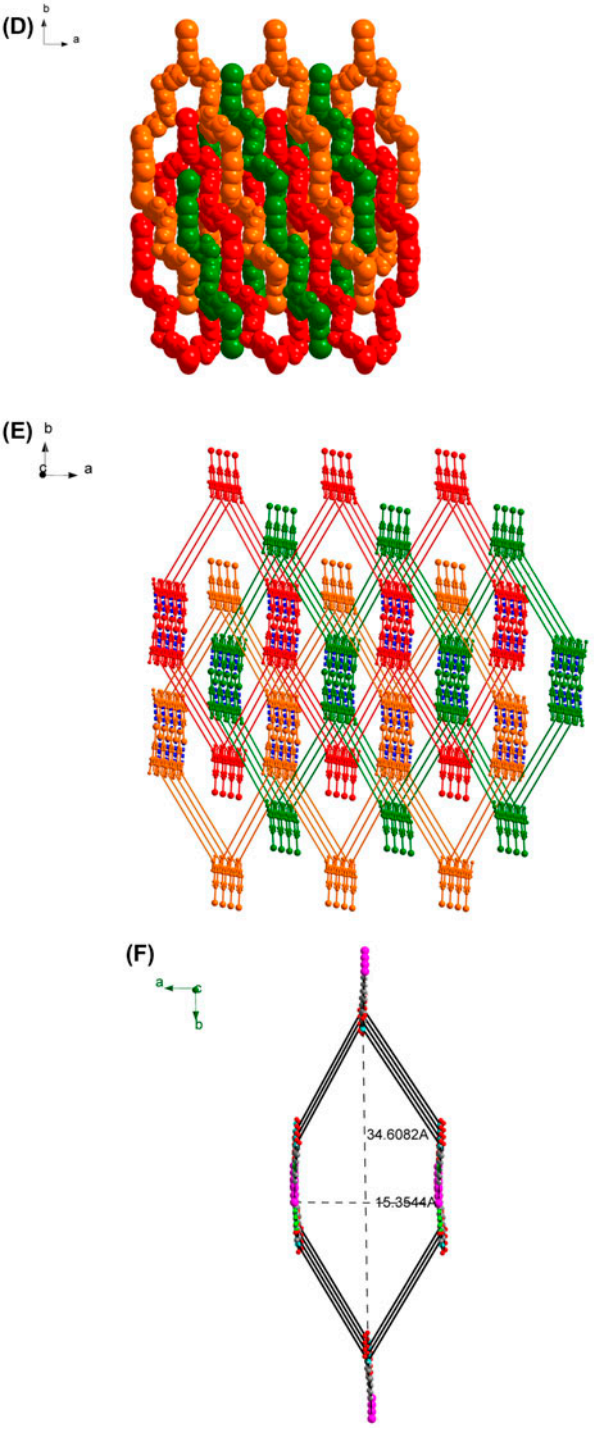

Figure 2. (*Continued*)

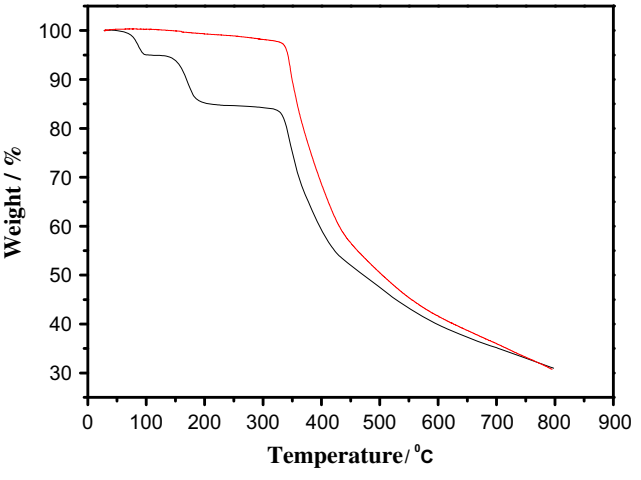

Figure 3. TGA curves of SWCPNT-**1** (black) and **2** (red) (see http://dx.doi.org/10.1080/00958972.2014.926006 for color version).

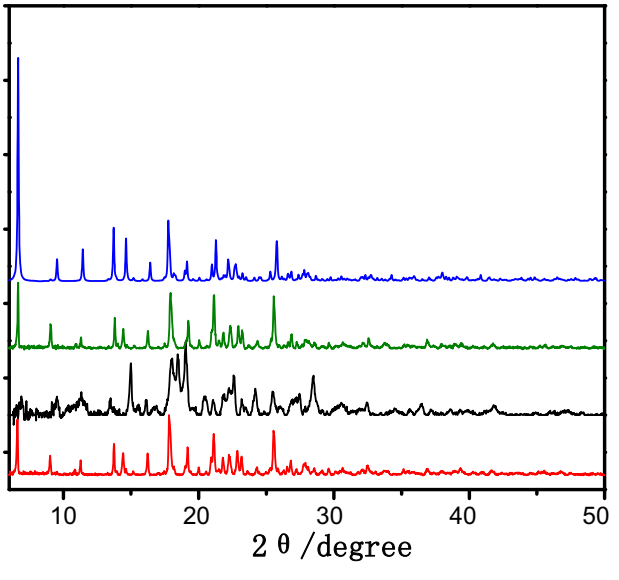

Figure 4. XRPD patterns for SWCPNT-**1** recorded (red) as-synthesized SWCPNT-**1** measured at room temperature, (black) after removal of the water at 105 °C, (green) after exposure of the desolvated material in static air at room temperature, and (blue) the simulated XRPD pattern calculated from single-crystal data of SWCPNT-**1** with Mercury 1.4.2 (see http://dx.doi.org/10.1080/00958972.2014.926006 for color version).

desolvated material is changed, as supported by the *in situ* variable temperature PXRD patterns. This observation clearly indicates that during the process of dehydration and rehydration in SWCPNT-**1**, the framework exhibits a novel "breathing" property which may mainly be attributed to the flexibility of the auxiliary ligand bbtz since the ligand IIP^{2-} is rigid.

The framework integrity of SWCPNT-**1** can be maintained after a number of desorption–adsorption cycles, which indicates that it may be used as potential adsorbent as well as sensing material to water molecules.

3.5. *Sorption to gasses*

Further, gas sorption (N_2 and CO_2) of the dehydrated **SWCPNT-1** was performed at 278.15 K. The N_2 adsorption isotherm at 278.15 K shows almost no uptake capacity, with the maximum of 0.9 mg at 38 atm. Interestingly, in the case of CO_2 desorption at 278.15 K, notable hysteresis loop was observed (figure 5). The sorption measurement of the dehydrated **SWCPNT-1** for CO_2 gave type-I isotherm for microporous materials, and the uptake at 38 atm is 13.2 mg g^{-1}, indicating that the dehydrated **SWCPNT-1** shows selective weak gas adsorption for CO_2 over N_2 at ambient temperature, which may be attributed to the smaller kinetic diameters of CO_2 than that of N_2 (CO_2 : 3.3; N_2 : 3.6 Å) as well as the significant quadrupole moment of CO_2 (-1.4×10^{-39} cm^2), which generates specific interactions with the host framework [62].

3.6. *Fluorescent properties in the solid state*

The photoluminescent spectra of SWCPNT-**1**, dehydrated SWCPNT-**1** (two H_2O molecules removed by heating at 105 °C for 6 h), **2**, and free H_2IIP acid have been investigated in the solid state at room temperature. To compare well the relative fluorescent intensities, we determined all of the emission spectra with the same excitation wavelength. Excitation of the microcrystalline samples SWCPNT-**1**, dehydrated SWCPNT-**1** and **2** at $\lambda_{ex} = 290$ nm leads to the generation of similar blue fluorescent emissions with the maximum emission centered around 469 nm and a shoulder at about 403 nm (figure 6). To further understand the origin of these emission bands, the fluorescent spectrum of free H_2IIP acid has also been

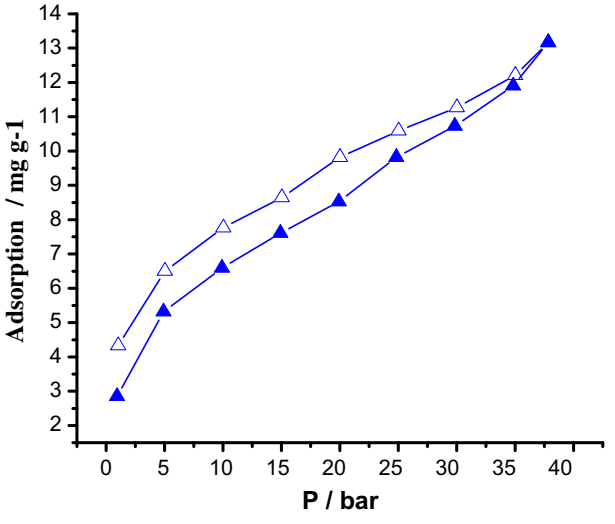

Figure 5. Sorption isotherm for SWCPNT-**1** to CO_2 measured at 278.15 K (solid: adsorption; blank: desorption).

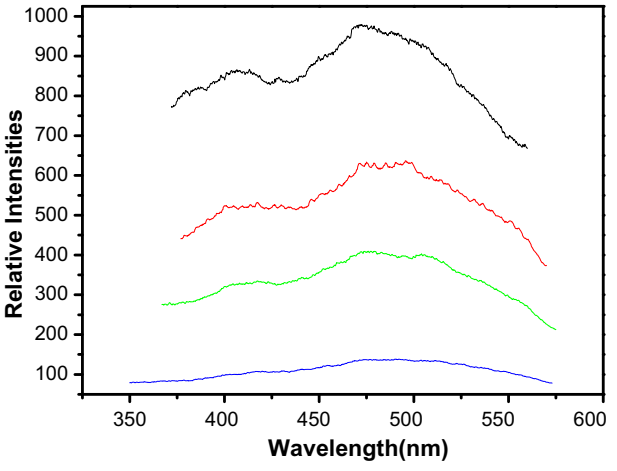

Figure 6. Solid-state fluorescence emissions recorded at room temperature for H_2IIP (blue), SWCPNT-**1** (red), the dehydrated SWCPNT-**1** (black) and **2** (green) (λ_{ex} = 290 nm) (see http://dx.doi.org/10.1080/00958972.2014.926006 for color version).

measured. The free H_2IIP acid exhibits the same maximum fluorescent emission and shoulder as those in SWCPNT-**1**, the dehydrated SWCPNT-**1** and **2**. These observations suggest that the coordination of the IIP^{2-} ligand with Zn(II) ion in the presence of bbtz as auxiliary ligands has almost no influence on the emission mechanism of SWCPNT-**1**, the dehydrated SWCPNT-**1** and **2**. So, the emissions of these complexes may be assigned to an intraligand $\pi\cdots\pi^*$ transition [63, 64]. The enhancement of fluorescence in SWCPNT-**1**, the dehydrated SWCPNT-**1** and **2** may be attributed to the ligation of the ligand to the Zn(II) center, which further enhances the rigidity of the IIP^{2-} ligand and reduces the loss of energy through a radiationless pathway [65, 66]. It is said that increasing molecular rigidity will weaken the intramolecular vibrations, so the molecule excitation energy is not easily released as heat due to vibration. The fluorescent emission of **2** is weaker compared with those of SWCPNT-**1** and the dehydrated SWCPNT-**1**, which is possibly attributed to the less rigid 2-D network architecture of **2** [67–69]. After removal of two water molecules, the emission of the dehydrated SWCPNT-**1** becomes much stronger than that of SWCPNT-**1**, indicating that the two water molecules in SWCPNT-**1** have great influence on its fluorescent intensity. The strong blue emission of the dehydrated SWCPNT-**1** reveals that this complex may be an excellent candidate for solid blue fluorescent material.

4. Conclusion

In conclusion, the present study not only shows that temperature as well as the cosolvent have great influence on the supramolecular assembly between the ligand IIP^{2-} and Zn(II) ion but also reveals that it is an effective strategy that the discrete single-walled Zn(II)-organic coordination polymer nanotube can be created by connecting the 0-D elliptical dimeric nanosized subunits through the rigid ligand IIP^{2-}. Based on this tactic, the unique fascinating discrete single-walled Zn(II)-organic coordination polymer nanotube SWCPNT-**1** was obtained under ambient condition in the presence of DMF as cosolvent, whilst a threefold-interpenetrated

3-D supramolecular network **2** was prepared under solvothermal condition at 120 °C in the presence of ethanol as cosolvent. The different conformations of bbtz ligand in these two complexes may mainly be induced by different temperatures and should be mainly responsible for the different architectures of SWCPNT-**1** and **2**. Both the coordinated and interstitial water molecules in SWCPNT-**1** can be completely removed without collapse of the tube. The most interesting property of SWCPNT-**1** is its rapid and reversible dehydration–rehydration behavior just in air. SWCPNT-**1** may be useful as potential late-model water adsorbent material. The dehydrated SWCPNT-**1** shows selective weak gas adsorption to CO_2 over N_2 and can also adsorb methanol and ethanol vapor weakly. The compounds, SWCPNT-**1** and the dehydrated SWCPNT-**1** and **2**, have been found to exhibit blue fluorescence in the solid state. Furthermore, the water molecules in SWCPNT-**1** have great influence on its fluorescent property. Further work is in progress to construct other novel MONTs based on H_2IIP in the presence of appropriate flexible auxiliary ligands.

Supplementary material

Crystallographic data have been deposited with the Cambridge Crystallographic Data Center with Nos. 813814 (SWCPNT-**1**) and 832542 (**2**). Copies of the data can be obtained free of charge via the Internet at http://www.ccdc.cam.ac.uk/conts/retrieving.html.

Acknowledgment

We gratefully acknowledge the Natural Science Foundation of Jiangsu Province (BK2012680), the Priority Academic Program Development of Jiangsu Higher Education Institutions (PAPD), the Key Laboratory of Environmental Material and Environmental Engineering of Jiangsu Province and the Analysis Center of Yangzhou University.

References

[1] S. Lijima. *Nature*, **354**, 56 (1991).
[2] W. Tremel. *Angew. Chem., Int. Ed.*, **38**, 2175 (1999).
[3] J. Chen, H.Y. Liu, W.A. Weimer, M.D. Halls, D.H. Waldeck, G.C.B. Walker. *J. Am. Chem. Soc.*, **124**, 9034 (2002).
[4] A. Harada, J. Li, M. Kamachi. *Nature*, **364**, 516 (1993).
[5] T.D. Clark, J.M. Buriak, K. Kobayashi, M.P. Isler, D.E. McRee, M.R. Ghadiri. *J. Am. Chem. Soc.*, **120**, 8949 (1998).
[6] D.T. Bong, T.D. Clark, J.R. Granja, M.R. Ghadiri. *Angew. Chem., Int. Ed.*, **40**, 988 (2001).
[7] B. Chen, Y. Ji, M. Xue, F.R. Fronczek, E.J. Hurtado, J.U. Mondal, C. Liang, S. Dai. *Inorg. Chem.*, **47**, 5543 (2008).
[8] Q.R. Fang, G.S. Zhu, M. Xue, J.Y. Sun, F.X. Sun, S.L. Qiu. *Inorg. Chem.*, **45**, 3582 (2006).
[9] A. Datcu, N. Roques, V. Jubera, D. Maspoch, X. Fontrodona, K. Wurst, I. Imaz, G. Mouchaham, J.P. Sutter, C. Rovira, J. Veciana. *Chem. Eur. J.*, **18**, 152 (2012).
[10] B. Li, S.Q. Zang, C. Ji, H.W. Hou, T.C.W. Mak. *Cryst. Growth Des.*, **12**, 1443 (2012).
[11] I. Grobler, V.J. Smith, P.M. Bhatt, S.A. Herbert, L.J. Barbour. *J. Am. Chem. Soc.*, **120**, 8949 (1998).
[12] A.C. McKinlay, R.E. Morris, P. Horcajada, G. Férey, R. Gref, P. Couvreur, C. Serre. *Angew. Chem., Int. Ed.*, **49**, 6260 (2010).
[13] O.M. Yaghi, M. O'Keeffe, N.W. Ockwig, H.K. Chae, M. Eddaoudi, J. Kim. *Nature*, **423**, 705 (2003).
[14] S. Kitagawa, R. Kitaura, S. Noro. *Angew. Chem., Int. Ed.*, **43**, 2334 (2004).
[15] J.T. Hupp, K.R. Poeppelmeier. *Science*, **309**, 2008 (2005).
[16] Z.Z. Lu, R. Zhang, Y.Z. Li, Z.J. Guo, H.G. Zheng. *J. Am. Chem. Soc.*, **133**, 4172 (2011).

[17] B. Zhao, P. Cheng, Y. Dai, C. Cheng, D.Z. Liao, S.P. Yan, Z.H. Jiang, G.L. Wang. *Angew. Chem., Int. Ed.*, **42**, 934 (2003).
[18] K.L. Zhang, Y. Chang, C.T. Hou, R. Wu, G.W. Diao, S.W. Ng. *CrystEngComm.*, **12**, 1194 (2010).
[19] F.N. Dai, H.Y. He, D.F. Sun. *J. Am. Chem. Soc.*, **130**, 14064 (2008).
[20] X.L. Wang, C. Qin, E.B. Wang, Y.G. Li, Z.M. Su, L. Xu, L. Carlucci. *Angew. Chem., Int. Ed.*, **44**, 5824 (2005).
[21] Y.J. Dong, Y.Y. Jiang, J.P. Ma, F.L. Liu, J. Li, B. Tang, R.Q. Huang, S.R. Batten. *J. Am. Chem. Soc.*, **129**, 4520 (2007).
[22] C.Y. Su, M.D. Smith, H.C. zur Loye. *Angew. Chem., Int. Ed.*, **42**, 4085 (2003).
[23] G.Z. Yuan, C.F. Zhu, Y. Liu, W.M. Xuan, Y. Cui. *J. Am. Chem. Soc.*, **131**, 10452 (2009).
[24] J. Xia, W. Shi, X.Y. Chen, H.S. Wang, P. Cheng, D.Z. Liao, S.P. Yan. *Dalton Trans.*, 2373 (2007).
[25] P. Jensen, S.R. Batten, B. Moubaraki, K.S. Murray. *Chem. Commun.*, 793 (2000).
[26] X.Y. Cao, J. Zhang, J.K. Cheng, Y. Kang, Y.G. Yao. *CrystEngComm.*, **6**, 315 (2004).
[27] S.B. Ren, X.L. Yang, J. Zhang, Y.Z. Li, Y.X. Zheng, H.B. Du, X.Z. You. *CrystEngComm.*, **11**, 246 (2009).
[28] H. Kitagawa, K. Otsubo. *Nat. Mater.*, **10**, 291 (2011).
[29] J. Fan, H.F. Zhu, T.A. Okamura, W.Y. Sun, W.X. Tang, N. Ueyama. *Inorg. Chem.*, **42**, 158 (2003).
[30] T. Panda, T. Kunduz, R. Banerjee. *Chem. Commun.*, **48**, 5464 (2012).
[31] T. Bataille, S. Bracco, A. Comotti, F. Costantino, A. Guerri, A. Ienco, F. Marmottini. *CrystEngComm.*, **14**, 7170 (2012).
[32] P. Thanasekaran, T.-T. Luo, C.-H. Lee, K.-L. Lu. *J. Mater. Chem.*, **21**, 13140 (2011).
[33] J.S. Seo, D. Whang, H. Lee, S.I. Jun, J. Oh, Y.J. Jeon, K. Kim. *Nature*, **404**, 982 (2000).
[34] M. Eddaoudi, J. Kim, N. Rosi, D. Vodak, J. Wachter, M. O'Keeffe, O.M. Yaghi. *Science*, **295**, 469 (2002).
[35] L. Pan, H. Liu, X. Lei, X. Huang, D.H. Olson, N.J. Turro, J. Li. *Angew. Chem., Int. Ed.*, **42**, 542 (2003).
[36] Z. Su, K. Cai, J. Fan, S.S. Chen, M.S. Chen, W.Y. Sun. *CrystEngComm.*, **12**, 100 (2010).
[37] S.S. Chen, M. Chen, S. Takamizawa, P. Wang, G.C. Lv, W.Y. Sun. *Chem. Commun.*, **47**, 4902 (2011).
[38] B. Wang, A.P. Côté, H. Furukawa, M. O'Keeffe, O.M. Yaghi. *Nature*, **453**, 207 (2008).
[39] E. Tang, Y.M. Dai, J. Zhang, Z.J. Li, Y.G. Yao, J. Zhang, X.D. Huang. *Inorg. Chem.*, **45**, 6276 (2006).
[40] F. Luo, S.R. Batten, Y.X. Che, J.M. Zheng. *Chem. Eur. J.*, **13**, 4948 (2007).
[41] F. Yu, X.J. Kong, Y.Y. Zheng, Y.P. Ren, L.S. Long, R.B. Huang, L.S. Zheng. *Dalton Trans.*, 9503 (2009).
[42] Y.Q. Lan, H.L. Jiang, S.L. Li, Q. Xu. *Inorg. Chem.*, **51**, 7484 (2012).
[43] V. Iancu, A. Deshpande, S.W. Hia. *Nano Lett.*, **6**, 820 (2006).
[44] S. Mosaoka, D. Tanaka, Y. Nakanishi, S. Kitagawa. *Angew. Chem., Int. Ed.*, **43**, 2530 (2004).
[45] X.S. Wang, S. Ma, P.M. Forster, D. Yuan, J. Eckert, J.J. Lopez, B.J. Murphy, J.B. Praise, H.C. Zhou. *Angew. Chem., Int. Ed.*, **47**, 7263 (2008).
[46] J. Wang, X. Qian, Y.-F. Cui, B.-L. Li, H.-Y. Li. *J. Coord. Chem.*, **64**, 2878 (2011).
[47] H.-W. Kuai, X.-C. Cheng, X.-H. Zhu. *J. Coord. Chem.*, **66**, 1795 (2013).
[48] G. Han, Y. Mu, D. Wu, Y. Jia, H. Hou, Y. Fan. *J. Coord. Chem.*, **65**, 3570 (2012).
[49] F. Yue, X. Yu, Y. Luo, J. Yang, X. Chen, H. Zhang. *J. Coord. Chem.*, **66**, 2843 (2013).
[50] J.-J. Wang, Q.-L. Bao, J.-X. Chen. *J. Coord. Chem.*, **66**, 2578 (2013).
[51] B. Liu, R. Wang, G. Jin, X.-R. Meng. *J. Coord. Chem.*, **66**, 1784 (2013).
[52] C. Janiak, L. Uehlin, H.P. Wu, P. Klęufers, H. Piotrowski, T.G. Scharmann. *J. Chem. Soc. Dalton Trans.*, 3121 (1999).
[53] K.L. Zhang, C.T. Hou, J.J. Song, Y. Deng, L. Li, S.W. Ng, G.W. Diao. *CrystEngComm.*, **14**, 590 (2012).
[54] K. Rissanen. *CrystEngComm.*, **10**, 1107 (2008).
[55] Y.F. Peng, B.Z. Li, J.H. Zhou, B.L. Li, Y. Zhang. *Cryst. Growth Des.*, **6**, 994 (2006).
[56] Y.F. Peng, B.Z. Li, J.H. Zhou, B.L. Li, Y. Zhang. *Chin. J. Struct. Chem.*, **23**, 985 (2004).
[57] G.M. Sheldrick. *SHELXL 97 Programs for Crystal Structure Analysis*, University of Götinggen, Germany (1997).
[58] A.L. Spek. *PLATON A Multipurpose Crystallographic Tool*, Utrecht University, Utrecht (2002).
[59] D. Eisenberg, W. Kauzmann. *The Structure and Properties of Water*, Oxford University Press, Oxford (1969).
[60] L. Carlucci, G. Ciani, D.M. Proserpio. *Coord. Chem. Rev.*, **246**, 247 (2003).
[61] K. Nakamoto. *Infrared and Raman Spectra of Inorganic and Coordination Compounds*, Wiley, New York (1986).
[62] S. Coriani, A. Halkier, A. Rizzo, K. Ruud. *Chem. Phys. Lett.*, **326**, 269 (2000).
[63] S.T. Wang, Y. Hou, E.B. Wang, Y.G. Li, L. Xu, J. Peng, S.X. Liu, C.W. Hu. *New J. Chem.*, **27**, 1144 (2003).
[64] S.J.A. Pope, B.J. Coe, S. Faulkner, E.V. Bichenkova, X. Yu, K.T. Douglas. *J. Am. Chem. Soc.*, **126**, 9490 (2004).
[65] S.L. Zheng, J.M. Yang, X.L. Yu, X.M. Chen, W.T. Wong. *Inorg. Chem.*, **43**, 830 (2004).
[66] S.L. Zheng, M.L. Tong, S.D. Tan, Y. Wang, J.X. Shi, Y.X. Tong, H.K. Lee, X.M. Chen. *Organometallics*, **20**, 5319 (2001).
[67] Y.Q. Huang, B. Ding, H.B. Song, B. Zhao, P. Ren, P. Cheng, H.G. Wang, D.Z. Liao, S.P. Yan. *Chem. Commun.*, **47**, 4906 (2006).
[68] L. Hou, Y.Y. Lin, X.M. Chen. *Inorg. Chem.*, **47**, 1346 (2008).
[69] H. Zhao, Z.R. Qu, H.Y. Ye, R.G. Xiong. *Chem. Soc. Rev.*, **37**, 84 (2008).